catalysts

MDPI

Article

Mechanistic Insights into Visible Light-Induced Direct Hydroxylation of Benzene to Phenol with Air and Water over Pt-Modified WO_3 Photocatalyst

Yuya Kurikawa [1], Masahiro Togo [1], Michihisa Murata [1], Yasuaki Matsuda [1], Yoshihisa Sakata [2], Hisayoshi Kobayashi [3] and Shinya Higashimoto [1,*]

1 Department of Applied Chemistry, Faculty of Engineering, Osaka Institute of Technology, 5-16-1 Omiya, Asahi-ku, Osaka 535-8585, Japan; m1m19508@st.oit.ac.jp (Y.K.); m1m19515@st.oit.ac.jp (M.T.); michihisa.murata@oit.ac.jp (M.M.); yasuaki.matsuda@oit.ac.jp (Y.M.)

2 Graduate School of Science and Technology for Innovation, Yamaguchi University, 2-16-1 Tokiwadai, Ube 755-8611, Japan; yoshi-sa@yamaguchi-u.ac.jp

3 Department of Chemistry and Materials Technology, Kyoto Institute of Technology, Matsugasaki, Sakyo-ku, Kyoto 606-8585, Japan; hisabbit@yahoo.co.jp

* Correspondence: shinya.higashimoto@oit.ac.jp; Tel.: +81-(0)6-6954-4283

Received: 2 May 2020; Accepted: 15 May 2020; Published: 18 May 2020

Abstract: Activation of C(sp2)-H in aromatic molecules such as benzene is one of the challenging reactions. The tungsten trioxide supported Pt nanoparticles (Pt-WO_3) exhibited hydroxylation of benzene in the presence of air and H_2O under visible-light ($420 < \lambda < 540$ nm) irradiation. The photocatalytic activities (yields and selectivity of phenol) were studied under several experimental conditions. Furthermore, investigations of mechanistic insight into hydroxylation of benzene have been carried out by analyses with apparent quantum yields (AQY), an $H_2{}^{18}O$ isotope-labeling experiment, kinetic isotope effects (KIE), electrochemical measurements and density functional theory (DFT) calculations. It was proposed that dissociation of the O–H bond in H_2O is the rate-determining step. Furthermore, the substitution of the OH derived from H_2O with H abstracted from benzene by photo-formed H_2O_2 indicated a mechanism involving a push-pull process for the hydroxylation of benzene into phenol.

Keywords: Pt-WO_3 photocatalyst; visible light; hydroxylation of benzene; phenol formation; isotope $H_2{}^{18}O$-labeling

1. Introduction

Visible light-driven photocatalysts for environmental conservation, securing energy resources and selective organic synthesis have received considerable attention because they can utilize unlimited solar energy [1–7]. Tungsten trioxide (WO_3) is one of the promising visible-light responsible photocatalyst having a direct band-gap excitation at ca. 2.7 eV. Recently, WO_3 has been proven to be an effective strategy for improving the photocatalytic degradation of volatile organic compounds (VOCs) such as acetaldehyde [8–11], toluene [12], acid [13]; water splitting to form O_2 in the presence of sacrificial agent [1]; as well as selective organic conversion such as oxidation of alcohol [14].

Phenols are important precursors for many chemicals and industrial products such as dyes and polymers, and they are currently produced from benzene by a three step cumene process. The cumene process for phenol formation exhibits low activity (~5% yield of phenol) and emission of large amounts of waste although the reactions require high temperature, high pressure and strong acidic conditions. Therefore, it is a great challenge to develop a one-step synthesis of phenol from benzene by using homogeneous and heterogeneous inorganic catalysts such as palladium membrane, titanium-containing

mesoporous molecular sieves and vanadium-substituted phosphomolybdate by hydrogen peroxide (H_2O_2) [15–17]. Although H_2O_2 is often used as environmentally friendly oxidant only to produce H_2O in catalytic hydroxylation of benzene, O_2 is more ideal oxidant than H_2O_2 due to its abundance in nature.

In a recent study, one-step direct hydroxylation of benzene toward phenol has been extensively studied using homogeneous photocatalysts such as quinolinium ions and $[Ru^{II}(Me_2phen)_3]^{2+}$ ions, [18–21], and heterogeneous semiconductor photocatalyst such as TiO_2 [22–27] and WO_3 [28,29] have been employed for selective photocatalytic hydroxylation of benzene to phenol under photo-irradiation ultraviolet (UV) light and/or visible-light. Yoshida et al. previously reported that platinum (Pt)-loaded TiO_2 (Pt-TiO_2) photocatalyst exhibited direct hydroxylation of benzene to form phenol and H_2 in the absence of O_2 under UV-light irradiation [22]. Also, Tomita et al. reported that the Pt-deposited WO_3 (Pt-WO_3) photocatalyst exhibited selective hydroxylation of benzene to phenol in the presence of O_2 and H_2O under light irradiation of both UV light and visible light ($300 < \lambda < 500$ nm) [28,29]. It was also confirmed that OH derived from H_2O is included in phenol by employing an $H_2{}^{18}O$ labeling experiment [29]. However, in a previous study, photocatalytic activities and reaction mechanisms for hydroxylation of benzene on the Pt-WO_3 have not been demonstrated under only irradiation of visible-light ($\lambda > 420$ nm).

In this study, we focus on understanding the photocatalytic activities for hydroxylation of benzene on the Pt-WO_3 photocatalyst under irradiation of only visible light ($420 < \lambda < 540$ nm). Furthermore, investigation of mechanistic insight has been carried out by combination with apparent quantum yields (AQY), $H_2{}^{18}O$ isotope labeling experiment, kinetic isotope effects (C_6D_6, D_2O), electrochemical measurements and density functional theory (DFT) calculations.

2. Results

2.1. Preparation of Pt-Deposited Tungsten Trioxide (WO_3) and Its Characterization

The Pt-WO_3 photocatalyst was characterized by X-ray diffraction (XRD), ultraviolet–visible (UV–Vis) spectroscopy, scanning transmittance electron microscope with energy-dispersed X-ray emission spectroscopy (STEM-EDS) and X-ray photoelectron spectroscopy (XPS) measurements. The XRD patterns of WO_3 and Pt-WO_3 were identified with a monoclinic structure in accordance with standard XRD profile of JCPDS cards No. 43-1035, and no other phase of Pt species was observed (see Figure 1 [I]). The WO_3 exhibited absorption spectrum in the visible-light region. Bandgap of the WO_3 was estimated to be ca. 2.6 eV from tauc plots υof $(F(R) \times h\upsilon)^2$ vs. $h\upsilon$ (See Figure S1). Furthermore, the Pt-WO_3 with different amounts of Pt species exhibited optical absorbance above 450 nm, which is attributable to the scattering effects from the Pt particles [30] or surface resonance [31]. The optical absorbance significantly increased as an increase of the Pt species deposited on the WO_3 (See Figure 1 [II]). The scanning transmittance electron microscope with the STEM-EDS image of Pt(0.4)-WO_3 confirmed that Pt nano-particles were dispersed on the WO_3 surface (See Figure 1 [III]). The XPS analysis indicated that the Pt(0.4)-WO_3 photocatalyst was observed to possess two different types of doublet peaks ($4f_{5/2}$ and $4f_{7/2}$) at 74.8 and 71.6 eV for Pt^0 as a major species, at 75.8 and 72.5 eV for Pt^{2+} as a minor species (See Figure 1 [IV]). These results indicated that Pt nano-particle deposition on the WO_3 was successfully performed by photo-electrochemical deposition methods.

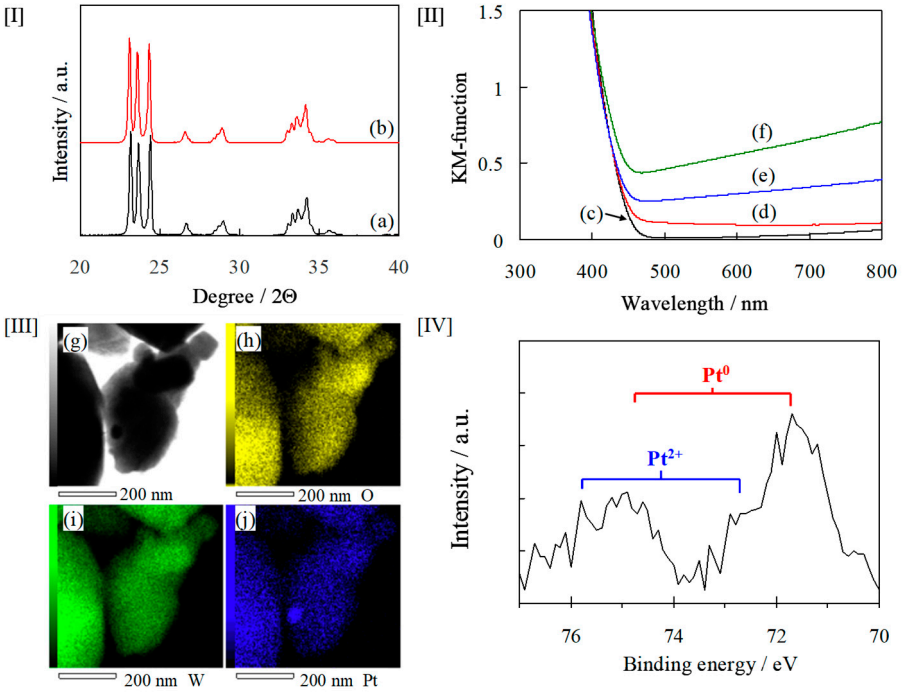

Figure 1. X-ray diffraction (XRD) patterns **[I]** of tungsten trioxide (WO_3) (a) and Pt(0.4)-WO_3 (platinum-tungsten trioxide) (b); ultraviolet–visible (UV–Vis) absorption spectra **[II]** of WO_3 (c), Pt(0.1)-WO_3 (d), Pt(0.2)-WO_3 (e), Pt(0.4)-WO_3 (f); scanning transmittance electron microscope (STEM) image (g) and energy-dispersed X-ray emission spectroscopy (EDS) (h–j) **[III]** of the Pt(0.4)-WO_3: O (h), W (i) and Pt (j); and XPS **[IV]** of Pt (4f) of the Pt(0.4)-WO_3.

2.2. *Photocatalytic Hydroxylation of Benzene on the Pt-WO_3 under Visible-Light Irradiation*

The photocatalytic hydroxylation of benzene in the presence of air and H_2O was performed on the WO_3 photocatalyst under visible-light irradiation. It was confirmed that the hydroxylation reaction does not take place under photo-irradiation without a photocatalyst nor with a photocatalyst without irradiation, i.e., both photocatalyst and irradiation are required in combination for hydroxylation reaction to occur. The WO_3 exhibited very low activity for phenol formation under visible-light irradiation (See Table S1). After the photocatalytic reaction, the color of suspension was slightly bluish, suggesting that the WO_3 was partially reduced and the ability for oxygen reductive reaction (ORR) was retarded. On the other hand, Pt-WO_3 exhibited significant improvement of photocatalytic activities for the formation of hydroxylated products such as phenol and catechol. The yields of phenols significantly improved as an increase of loading amounts of Pt species up to 0.2 atom%, and the activity was saturated at 0.4 atom%. The selectivity of phenol was optimized at 0.1 atom% and then slightly decreased as an increase of Pt-deposition (see Figure 2 [I], Table S1). Reaction time profile for phenol evolution on the Pt(0.2)-WO_3 photocatalyst was shown in Figure 2 [II]. The photocatalytic activity increased as an increase of reaction time: producing 29 μmol of phenol with 47 % selectivity after photocatalytic reaction for 20 h, and 40 μmol phenol with 64% selectivity for 70 h. (See distribution of side products shown in Table S2). After the reaction for 70 h, the amount of photo-formed H_2O_2 was only 0.15 μmol, which are much less than hydroxylated products assuming two electron reduction of O_2 to form H_2O_2. It can be considered that the H_2O_2 may be self-decomposed on the photocatalyst and/or participate in the reaction for the hydroxylation of benzene. The role of H_2O_2 will be discussed later. Moreover, when the volume of solvent in the reaction became small, the yields of phenol decreased, while the selectivity of phenol improved over 70% (See Table S3). Therefore, a trade-off relation between the yields and selectivity of phenol was observed. The surface coverage of the photocatalyst by condensation of the adsorbent could be considered to prevent over oxidation of benzene leading

to high selectivity of phenol, of which the similar phenomena was previously reported on the TiO_2 photocatalyst [25].

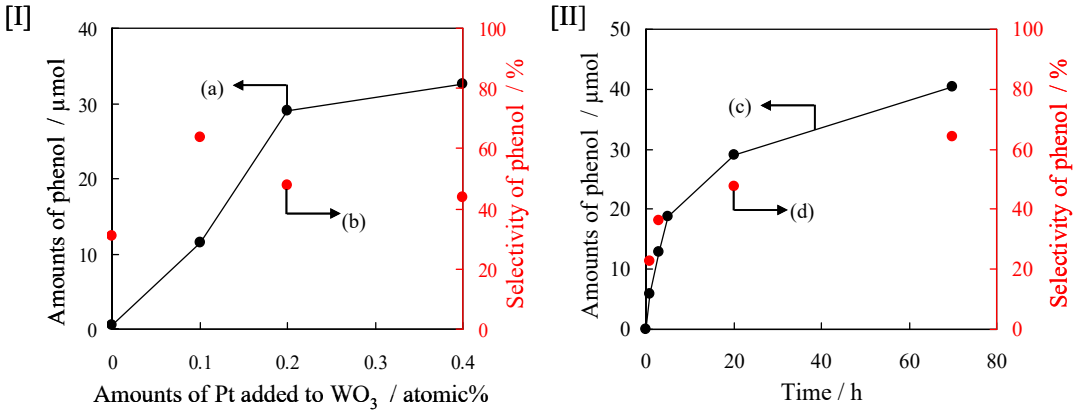

Figure 2. Dependence of loading amounts of Pt deposited on the WO_3 [**I**]; and reaction time profile on the Pt(0.2)-WO_3 [**II**] for hydroxylation of benzene to form phenol (yields: a, c; and selectivity: b and d) under visible-light irradiation.

Apparent quantum yields (AQY) on the Pt(0.2)-WO_3 were measured. Assuming one photon producing one phenol, the AQY for phenol formation reached over 2% by excitation at 400 nm as shown in Figure 3. The AQY profile was found to be very similar with the absorption spectrum of WO_3, suggesting that phenol formation is strongly correlated with the light absorbance of WO_3, not with Pt scattering [30] and/or resonance absorbance [31].

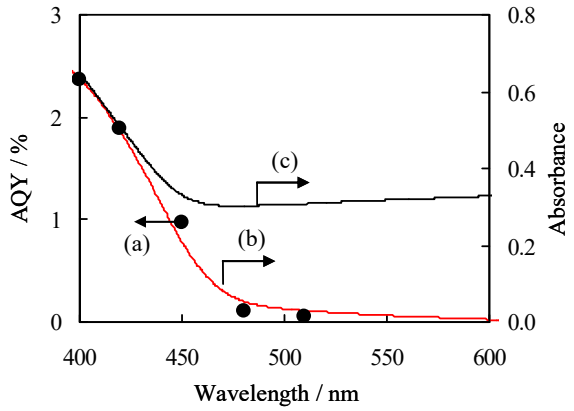

Figure 3. Dependence of wavelength photo-irradiated on apparent quantum yields, AQY (a) for hydroxylation of benzene to phenol, and UV–Vis absorbance of WO_3 (b) and Pt(0.2)-WO_3 (c).

2.3. Role of H_2O on the Photocatalytic Reactions

In order to understand role of H_2O, the $H_2{}^{18}O$-labeling experiments for photocatalytic hydroxylation of benzene were performed by liquid chromatography–mass spectrometry (LC-MS), and results are shown in Table 1 and Figure S2. It is noted that the atomic exchanges between O_2 and H_2O, and between O_2 and phenol are very slow even under photo-irradiation [23,32]. Therefore, $H_2{}^{18}O$ was used for tracing O species incorporated in phenol. When the photocatalytic reactions were carried out in the presence of $H_2{}^{16}O$ (100%), the photo-formed phenol was only observed at the mass number of 93 (*m*/*z*), which is attributed to the phenolic anion ($C_6H_5{}^{16}O^-$). Furthermore, when the photocatalytic reactions by employing $H_2{}^{16}O$ (90%)/$H_2{}^{18}O$ (10%) were carried out, the peaks at 93 (*m*/*z*) for the $C_6H_5{}^{16}O^-$ as well as 95 (*m*/*z*) for $C_6H_5{}^{18}O^-$ were observed. The peak intensities indicated that the ratio of ^{18}O to ^{16}O involved in the photo-formed phenol was 9.9% under visible-light

(420 < λ < 540 nm), while 9.1% under UV-light irradiation (300 < λ < 400 nm). Assuming that $H_2{}^{16}O$ and $H_2{}^{18}O$ exhibited same activity for hydroxylation of benzene, it was concluded that hydroxyl groups in phenol is almost derived from H_2O under both irradiation of visible-light and UV-light.

Table 1. $H_2{}^{18}O$ isotope labeling test for photocatalytic hydroxylation of benzene on the Pt(0.2)-WO_3.

Entry	Products/μmol							$^{18}O/^{16}O$ [1] Ratios in Phenol/%
	PH	RE	BQ	CA	HQ	PL	PG	
1	22.0	1.4	0.01	4.3	0.1	3.4	1.9	9.9
2	18.0	0.4	0.03	5.9	1.3	5.5	1.7	9.1

[1] $H_2{}^{16}O$ (90%)/$H_2{}^{18}O$ (10%) (5 mL), benzene: 300 μmol, visible-light irradiation (entry 1) and UV-light irradiation (entry 2) for 20 h. Abbreviation: phenol (PH), resolcinol (RE), *p*-benzoquinone (BQ), catechol (CA), hydroquinone (HQ), phloroglucinol (PL), pyrogallol (PG).

The rate determining step for hydroxylation of benzene was investigated by the kinetic isotope effect (KIE) using D_2O and C_6D_6 (See Figure 4). The reaction rate constants for formation of phenol from normal benzene (C_6H_6) in the presence of H_2O and D_2O were roughly estimated to be 3.75×10^{-6} and 1.42×10^{-6} s^{-1} for (a) and (b), respectively. The kinetic isotope effect (k_{H2O}/k_{D2O}) was estimated to be ca. 2.7 (see Figure 4 [I]). On the other hand, the reaction rate constants for formation of phenol from C_6H_6 and C_6D_6 in the presence of H_2O were roughly estimated to be 3.75×10^{-6} and 3.77×10^{-6} s^{-1} for (c) and (d), respectively. That is, the KIE of k_{C6H6}/k_{C6D6} was estimated to be 1.0 (see Figure 4 [II]). These results suggest that the dissociation of O–H bond in the H_2O plays an important role in the rate determining step for the hydroxylation of benzene.

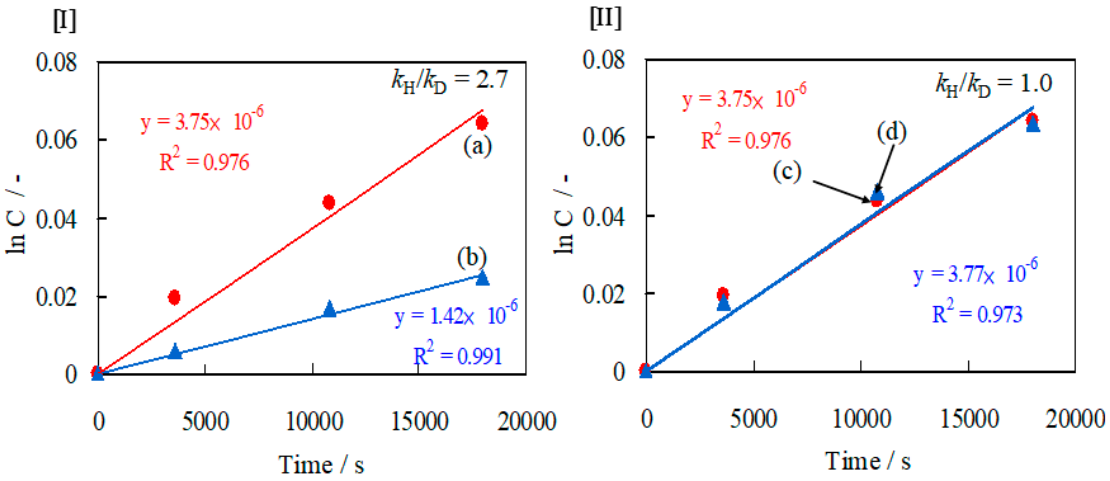

Figure 4. Kinetic isotope effects (KIE) on photocatalytic hydroxylation of benzene in the presence of air and H_2O on Pt(0.2)-WO_3 (20 mg) under visible light irradiation. Hydroxylation of C_6H_6 in the presence of H_2O (a) and D_2O (b) [**I**]; and that of C_6H_6 (c) and C_6D_6 (d) in the presence of H_2O [**II**].

2.4. Role of O_2 on the Photocatalytic Reactions

When the half reaction for the photocatalytic hydroxylation of benzene was performed on the Pt-WO_3 in the presence of Ag^+ ions as electron scavenger instead of O_2 under visible-light irradiation, no products could be detected under visible-light irradiation (Table 2). This result indicated that both H_2O and O_2 (air) in combination are essential for hydroxylation of benzene under visible-light irradiation.

Table 2. Effects of Ag^+ ions added on the photocatalytic hydroxylation of benzene on the Pt(0.2)-WO_3 photocatalyst under photo-irradiation.

Reaction Condition	Products/μmol							Selectivity of PH/%
	PH	RE	*p*-BQ	CA	HQ	PL	PG	
Visible light/air	29.0	1.2	0.2	18.3	0.3	19.0	2.4	41.0
Visible light/N_2 (1)	0	0	0	0	0	0	0	-
UV light/N_2 (1)	1.1	0.5	0.5	0.6	0.2	6.8	0.06	11.7

(1) presence of Ag^+ (50 μmol) under N_2 purge.

The flat band potential of WO_3 was obtained from capacitance versus voltage measurements. The WO_3 powder was deposited on fluorine-doped tin oxide (FTO) coated glass. Mott–Schottky plots indicated that the flatband potential (≈conduction band) of the WO_3/FTO was estimated to be +0.40 V vs. reversible hydrogen electrode (RHE) (Figure S3). LSV measurements of WO_3 and Pt-WO_3 were carried out in O_2-saturated 0.1 M Na_2SO_4 aq. The cathodic current was obtained at the potential more cathodic than the conduction band (+0.40 V vs. RHE) of WO_3 (See Figure S4). This cathodic current would be attributed to the reduction of WO_3. Furthermore, the cathodic current significantly increased by deposition of Pt on WO_3. A deposition of Pt species as a co-catalyst caused an improvement of the ORR. It is noted that multi-electron reduction of O_2 to H_2O_2, thermodynamically occurred at $E^0(O_2/H_2O_2)$ = +0.68 V [33]. An increase of cathodic current is attributed to the effective electron transfer to O_2 via Pt species to form H_2O_2 [34].

It was confirmed that the hydroxylation of benzene in the presence of H_2O_2 did not take place under photoirradiation without a photocatalyst nor with photocatalyst without irradiation. However, both photocatalyst and visible-light irradiation are required for the hydroxylation of benzene (See Table S4). In order to understand the role of H_2O_2, the hydroxylation of benzene (300 μmol) in the presence of H_2O_2 (150 μmol) and $H_2{}^{16}O$ (90%)/$H_2{}^{18}O$ (10%) was conducted on the Pt-WO_3 under visible-light irradiation. As a result, the ratio of ^{18}O to ^{16}O was determined to be 8.3%, suggesting that major contribution of OH groups in phenol came from H_2O even in the presence of H_2O_2.

2.5. Reaction Mechanisms for Photocatalytic Hydroxylation of Benzene to Phenol

In order to evaluate the oxidation power of photo-induced holes, photocatalytic half reactions on the Pt(0.2)-WO_3 photocatalyst were carried out. It was observed that addition of Ag^+ ions instead of O_2 showed no products under visible-light irradiation, while the phenolic compounds were detected under UV-light irradiation (See Table 2). These results suggest that water oxidation by UV-light irradiation induced strong oxidation power possibly to form free OH radicals, which would attack benzene directly [29], but by visible-light irradiation would not form OH radicals. In fact, we employed the tertiary butyl alcohol (TBA) as scavengers of OH radicals. As a result, the TBA added in the photocatalytic system on the Pt-WO_3 under visible-light irradiation did not influence to the yields of phenol (Table 3). However, the amounts of catechol (CA) and phloroglucinol (PL) decreased by the addition of TBA (See Table 3). The di- and tri- OH groups involved in phenolic compounds may be partially derived from O_2. Research is under way using an $^{18}O_2$ labeling test.

Table 3. Effects of tertiary butyl alcohol (TBA) added on the photocatalytic hydroxylation of benzene on the Pt(0.2)-WO_3 photocatalyst under visible light irradiation for 20 h under air.

TBA Added/μmol	Products/μmol							Selectivity of PH/%
	PH	RE	BQ	CA	HQ	PL	PG	
0	29.0	1.2	0.19	18.3	0.34	19	2.4	41.0
50	29.2	1.39	0.25	13.3	0.27	7.9	5.0	51.0

As mentioned above, H_2O_2 was confirmed to form as intermediate species by multi-electron reduction of O_2 during photocatalytic hydroxylation of benzene. The reaction mechanisms were investigated by DFT calculations. Figure 5 [Ia] showed the optimized structures of the reactant, transitional state (TS) and product by the interactions of benzene, H_2O with H_2O_2. The O–H bond length in H_2O, O–O in H_2O_2 and C–H in benzene were observed to increase through the reaction path. It was found that H_2O_2 could assist C-H bond dissociation from benzene. Subsequently, OH species derived from H_2O was incorporated within phenol in the final product. Moreover, the reaction path in the presence of the Pt co-catalyst was investigated (See Figure 5 [Ib]). Strong interaction of H_2O_2 with Pt_3 was observed to dissociate the O–O bond to form O species, and subsequently, the C–H bond in benzene was dissociated by an assist of the O species and/or Pt_3. The energy changes for overall reactions were indicated in Figure 5 [II]. The hydroxylation of benzene proceeded on much lower potential energy surface with the Pt_3 co-catalyst than that without Pt_3 co-catalyst. Thus, we have demonstrated the possible reaction path for hydroxylation of benzene to form phenol including OH groups derived from H_2O.

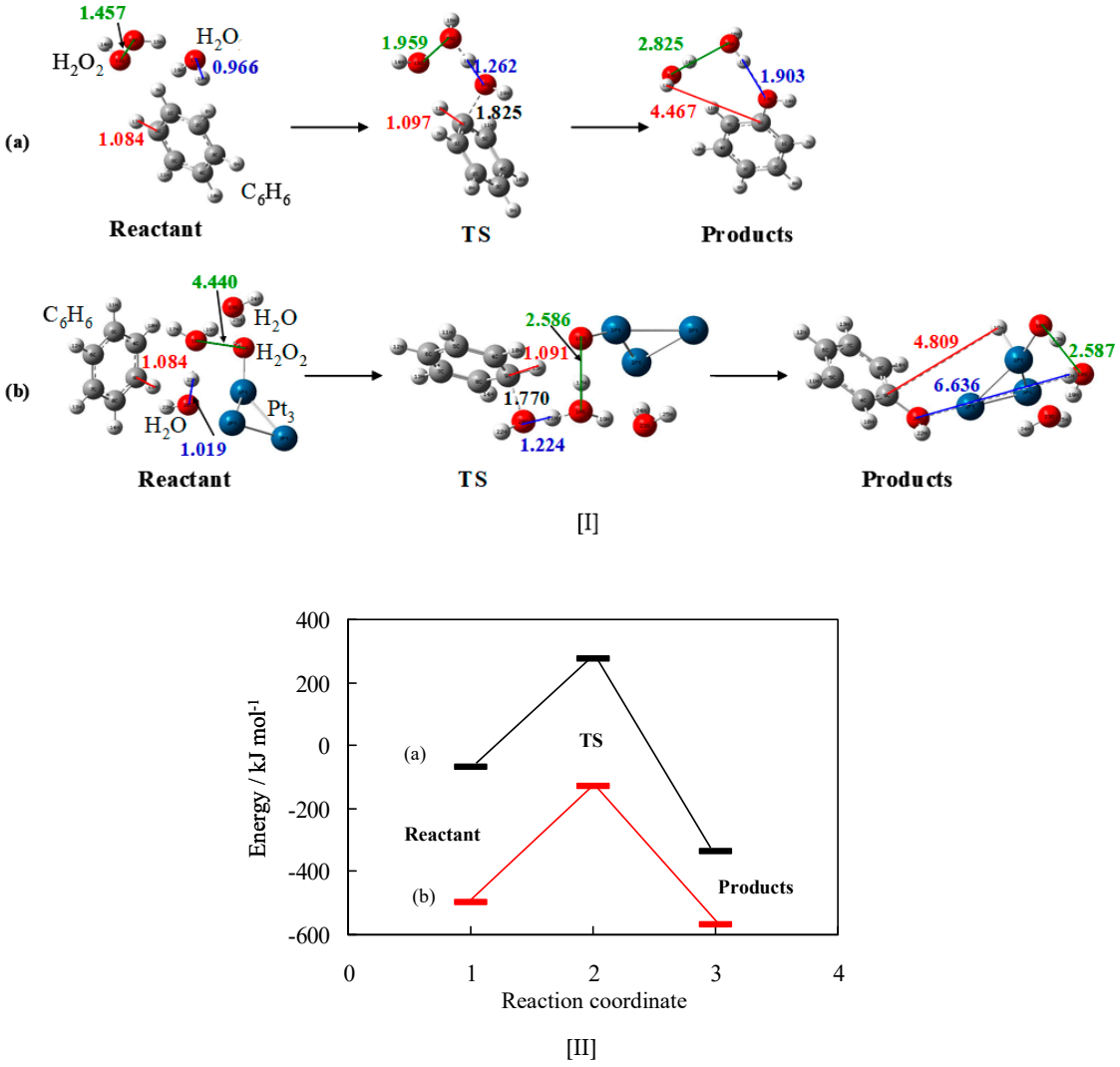

Figure 5. Optimized structures at the reactant, TS and product between benzene, H_2O and H_2O_2 system in the absence **[Ia]** and presence **[Ib]** of Pt_3 as co-catalyst for the hydroxylation of benzene to form phenol; and energy potentials for intrinsic reaction coordinates (IRC) **[II]**. The stabilization energy at each state was calculated by the difference from the energy of isolated system. The bond distance (Å) of O–H in H_2O (blue), O–O in H_2O_2 (green) and C–H in benzene (red) were indicated.

The reaction mechanism for the direct hydroxylation of benzene to phenol on the Pt-WO_3 was proposed (See Figure 6). This reaction is initiated by visible-light irradiation of the WO_3. The photo-induced holes and electrons are generated in the VB and CB of the WO_3, respectively. It was assumed that the photo-induced holes can oxidize H_2O to form O_2 [1], as well as activated $(H_2O)^*$ intermediate species of which the O–H bond length would be increased. On the other hand, the electrons effectively transfer from CB to O_2 via Pt species to form peroxide species such as H_2O_2, which would be further activated on the catalyst surface. The activated $(H_2O)^*$ species would attack the π electrons of the aromatic benzene ring, assisting the activated $(H_2O_2)^*$ to dissociate the C–H bond in benzene. It was, thus, proposed that the hydroxylation of benzene occurs by a mechanism involving a push-pull process, which promotes the formation of phenol.

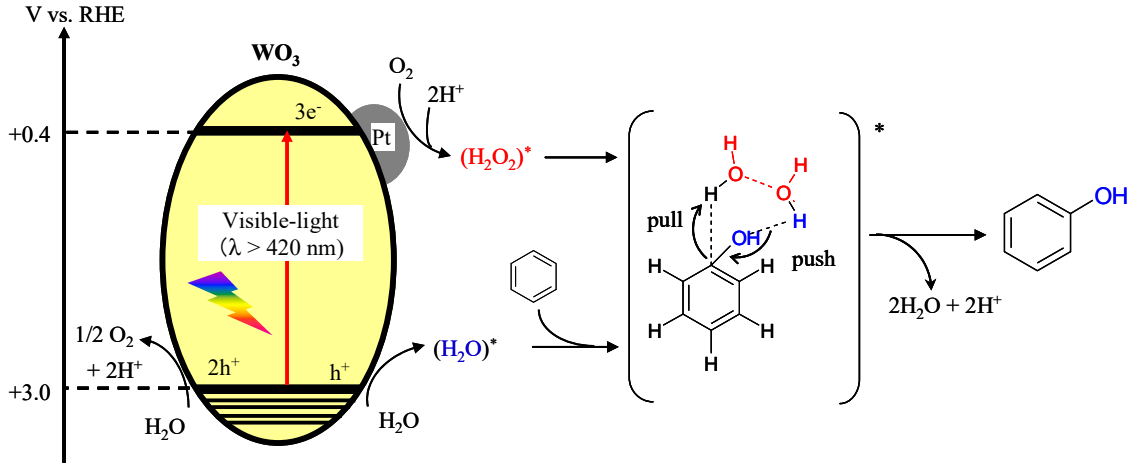

Figure 6. Reaction mechanisms for the hydroxylation of benzene into phenol in the presence of O_2 and H_2O on the Pt-WO_3 under visible light irradiation. (*) indicates formation of activated H_2O and H_2O_2 intermediates by photo-excitation.

3. Materials and Methods

3.1. Materials

Tungsten trioxide (WO_3, 99.9%) from Kojundo Chemical Laboratory (Osaka, Japan), $H_2PtCl_6{\cdot}6H_2O$ (99.9%) from Wako Pure Chemical Industries (Osaka, Japan); and water-^{18}O (97 atom% ^{18}O) and titanium (IV) oxysulfate solution (99.99%) from Sigma-Aldrich (St. Louis, MO, USA) were purchased. All chemicals were used without further purification.

3.2. Photoelectrochemical Deposition of Pt Species as Co-Catalyst on the WO_3

Photoelectrochemical deposition of Pt species was conducted on the WO_3 surface. WO_3 powder (1.0 g) was suspended in distilled water (25 mL) involving desired amounts of H_2PtCl_6 (4.32×10^{-6} ~ 2.16×10^{-5} mol), and the suspension was photo-irradiated by a light-emitting diode (LED) lamp ($420 < \lambda < 540$ nm) for 1 h under stirring in order to disperse photo-adsorbed Pt species. Subsequently, methanol (5 mL) as reductant was added into the suspension, and then it was continuously photo-irradiated for 4 h. The solid products were separated by centrifuge (LC-200, TOMY, 4500 rpm), followed by washing with distilled water and acetonitrile, and drying under vacuum condition at ambient temperature over night. The photocatalyst was referred to be as Pt(x)-WO_3(x: atom%). The photocatalyst was kept in the ambient temperature, and the photocatalytic reactions were carried out without further treatment of photocatalyst.

3.3. Characterizations

The X-ray diffraction (XRD) patterns were obtained with a RIGAKU RINT2000 using Cu K_α radiation (λ = 1.5417 Å) (RIGAKU, Tokyo, Japan). The oxidative states of Pt species were analyzed by an X-ray photoelectron spectroscope (XPS), KRATOS, AXIS Ultra, using Al K_α radiation (E = 1486.8 eV) (Shimadzu, Kyoto, Japan). The UV–Vis spectroscopic measurements were carried out on diffuse reflectance with a UV–Vis scanning spectrophotometer (UV-3100PC, Shimadzu, Kyoto, Japan). The elemental distribution images were taken with scanning transmittance electron microscope with energy-dispersed X-ray emission spectroscopy (STEM-EDS; JEOL JSM-2100, Tokyo, Japan).

3.4. Photocatalytic Reactions

Photocatalyst (20 mg) was suspended in distilled water (2, 5 or 10 mL) in a pyrex reaction tube (volume: 20 mL) under air capped with precision seal septum. If specific description was not given, the distilled water (10 mL) was introduced. And subsequently, 26.8 μL of benzene (300 μmol) was dropped into the suspension by a syringe under vigorous stirring. The reaction cell was photo-irradiated by a blue LED (visible light: $420 < \lambda < 540$ nm) or black light (UV light: $300 < \lambda < 400$ nm) at 298 K. The light energy intensities were shown in Figure S5. After the reaction, the catalysts were immediately separated from the suspension by filtration through a 0.20 μm membrane filter (Dismic-25JP, Advantec, Tokyo, Japan). The solution was, then, analyzed by High Performance Liquid Chromatography (HPLC, Shimadzu LC10ATVP, Kyoto, Japan, UV–Vis detector, column: Chemcopak, mobile phase: a mixture of acetonitrile and 1.0% formic acid aqueous solution), and several products were identified (see Figure S6). The gas phase (CO_2) was analyzed by Gas Chromatography–thermal conductivity detector (GC-TCD, Shimadzu GC-8A, Kyoto, Japan; column: porapak Q). Titanium sulfate (100 μL) was added to 1 mL of the reaction solution, and amounts of H_2O_2 formed in solution were analyzed by colorimetry from the value of absorbance at 410 nm in the UV–Vis absorption spectrum.

For the tracer experiment, $H_2{}^{18}O$ was used as the oxygen isotope source. The photocatalytic hydroxylation of benzene or phenol was carried out over Pt-WO_3 photocatalyst in the presence of $H_2{}^{18}O$ (10%)/$H_2{}^{16}O$ (90%) as solvent and air under visible-light irradiation for 20 h. The photocatalytic hydroxylation of benzene was performed in the presence of $H_2{}^{16}O_2$ (100 μmol) and $H_2{}^{18}O$ (10%)/$H_2{}^{16}O$ (90%) under visible-light irradiation for 2 h. Phenol in aqueous solutions were extracted by toluene, and the molar ratios of Ph-^{18}OH and Ph-^{16}OH were identified by LC-MS (Shimadzu LCMS-2020 spectrometer, Kyoto, Japan).

3.5. Electrochemical Measurements

Flatband potentials of the photoelectrodes were measured by a Potentio/Galvanostat (PGSTAT204, Autolab). The electrolysis cell was constructed with three electrodes, the WO_3 photoelectrode as working electrode, the platinum wire as auxiliary, and Ag/AgCl as the reference electrode. The WO_3 photoelectrodes were prepared as follows: the WO_3 (20 mg) was suspended in ethanol (0.2 mL) by a super-sonification to form a paste. The paste was then spread onto the FTO (active space 1.0 cm^2, Aldrich) by spin coating (2200 rpm, 30 s) for 3 times, followed by heat-treatment at 773 K for 1 h in air. Prior to measurements, 0.10 M Na_2SO_4 aqueous solution was vigorously bubbled by N_2 gas for 20 min in order to remove O_2.

Linear sweep voltammetry (LSV) was conducted at the rate of 10 mV s^{-1}. The photocatalyst (20 mg) was added into ethanol (0.2 mL), followed by a super-sonification for 5 min to disperse. The paste was casted by spin-coating (2200 rpm, 30 s) on the conductive transparent glass (FTO, 10 Ω/□, Sigma Aldrich, St. Louis, MO, USA) 3 times, followed by heat-treatment at 373 K overnight. Prior to LSV measurements, 0.10 M Na_2SO_4 aq. was vigorously bubbled by O_2 for 20 min.

3.6. Density Functional Theory (DFT) Calculation

Gaussian 09 program [35] and the hybrid B3LYP functional [36] were used. For Pt atoms, the Los Alamos effective core potentials [37] were employed along with the corresponding valence double basis sets [38]. For other atoms, a 6-311G(d,p) basis set was used. After the transition state (TS) was characterized, the intrinsic reaction coordinate (IRC) analysis [39] was carried out for both directions, reactant and product sides. The IRC analyses were followed by normal optimization runs, and the reactant and product were optimized as local minima.

4. Conclusions

In this study, we provided an understanding of photocatalytic activities for the hydroxylation of benzene under irradiation of only visible-light ($420 < \lambda < 540$ nm). It was demonstrated that hydroxylation of benzene on the Pt-WO_3 photocatalyst in the presence of air and H_2O produced several products such as phenol, catechol and phloroglucinol etc., and the selectivity of phenol improved over 70%.

One of novelties in our findings was to confirm the reaction mechanisms for photocatalytic hydroxylation of benzene into phenol by experimental and theoretical studies. An investigation of the mechanistic insights has been carried out by the combination with apparent quantum yields (AQY), an $H_2{}^{18}O$ isotope-labeling experiment, kinetic isotope effects (C_6D_6, D_2O), electrochemical measurements, and DFT calculations. It was proposed that the substitution of the OH derived from H_2O with H abstracted from benzene by photo-formed H_2O_2 indicated a mechanism involving a push-pull process for the hydroxylation of benzene into phenol. Our results showed new perspectives for the enhancement of yields and selectivity of phenol, as well as deeper understanding of the reaction mechanisms for the hydroxylation of benzene into phenol on the Pt-WO_3 photocatalyst.

Supplementary Materials: The following are available online at http://www.mdpi.com/2073-4344/10/5/557/s1: Figure S1: Tauc plots of WO_3, Figure S2: $H_2{}^{18}O$ isotope labeling experiments, Figure S3: Mott–Schottky plots of WO_3, Figure S4: LSV measurements of WO_3 and Pt-WO_3, Figure S5: Photo-intensities emitted from light-emitting diode (LED) and UV lamp, Figure S6: Molecular structures of products, Table S1: Photocatalytic activities depending on the amounts of Pt-deposition, Table S2: Time profiles in the photocatalytic reaction, Table S3: Effects of volumes in the reaction on the photocatalytic activity, Table S4: Role of H_2O_2 for the photocatalytic reactions.

Author Contributions: Conceptualization, S.H.; investigation, Y.K., M.T.; writing—original draft preparation, Y.K.; writing—review and editing, S.H., Y.S., H.K., M.M., Y.M.; supervision, S.H.; project administration, S.H. All authors have read and agreed to the published version of the manuscript.

Funding: This research received no external funding.

Conflicts of Interest: The authors declare no conflict of interest.

References

1. Wang, Y.; Suzuki, H.; Xie, J.; Tomita, O.; Martin, D.J.; Higashi, M.; Kong, D.R.; Abe, R.; Tang, J. Mimicking natural photosynthesis: Solar to renewable H_2 fuel synthesis by Z-scheme water splitting systems. *Chem. Rev.* **2018**, *118*, 5201–5241. [CrossRef] [PubMed]
2. Schneider, J.; Matsuoka, M.; Takeuchi, M.; Zhang, J.; Horiuchi, Y.; Anpo, M.; Bahnemann, D.W. Understanding TiO_2 photocatalysis: Mechanisms and materials. *Chem. Rev.* **2014**, *114*, 9919–9986. [CrossRef] [PubMed]
3. Ma, Y.; Wang, X.; Jia, Y.; Chen, X.; Han, H.; Li, C. Titanium dioxide-based nanomaterials for photocatalytic fuel generations. *Chem. Rev.* **2014**, *114*, 9987–10043. [CrossRef] [PubMed]
4. Kou, J.; Lu, C.; Wang, J.; Chen, Y.; Xu, Z.; Varma, R.S. Selectivity enhancement in heterogeneous photocatalytic transformations. *Chem. Rev.* **2017**, *117*, 1445–1514. [CrossRef] [PubMed]
5. Yamashita, H.; Mori, K.; Kuwahara, Y.; Kamegawa, T.; Wen, M.; Verma, P.; Che, M. Single-site and nano-confined photocatalysts designed in porous materials for environmental uses and solar fuels. *Chem. Soc. Rev.* **2018**, *47*, 8072–8096. [CrossRef]
6. Higashimoto, S. Titanium dioxide-based visible-light sensitive photocatalysis: Mechanistic insight and applications. *Catalysts* **2019**, *9*, 201. [CrossRef]

7. Asahi, R.; Morikawa, T.; Irie, H.; Ohwaki, T. Nitrogen-doped titanium dioxide as visible light-sensitive photocatalyst: Designs, developments, and prospects. *Chem. Rev.* **2014**, *114*, 9824–9852. [CrossRef]
8. Abe, R.; Takami, H.; Murakami, N.; Ohtani, B. Pristine simple oxides as visible light driven photocatalysts: Highly efficient decomposition of organic compounds over platinum-loaded tungsten oxide. *J. Am. Chem. Soc.* **2008**, *130*, 7780–7781. [CrossRef]
9. Arai, T.; Horiguchi, M.; Yanagida, M.; Gunji, T.; Sugihara, H.; Sayama, K. Reaction mechanism and activity of WO_3-catalyzed photodegradation of organic substances promoted by a CuO cocatalyst. *J. Phys. Chem. C* **2009**, *113*, 6602–6609. [CrossRef]
10. Arai, T.; Horiguchi, M.; Yanagida, M.; Gunji, T.; Sugihara, H.; Sayama, K. Complete oxidation of acetaldehyde and toluene over a Pd/WO_3 photocatalyst under fluorescent- or visible-light irradiation. *Chem. Commun.* **2008**, *43*, 5565–5567. [CrossRef]
11. Tomita, O.; Sugimoto, T.; Sako, K.; Hayakawa, S.; Katagiri, K.; Inumaru, K. Enhanced photocatalytic activity of Pt/WO_3 photocatalyst combined with TiO_2 nanoparticles by polyelectrolyte-mediated electrostatic adsorption. *Catal. Sci. Technol.* **2015**, *5*, 1163–1168.
12. Higashimoto, S.; Katsuura, K.; Yamamoto, M.; Tahakashi, M. Photocatalytic activity for decomposition of volatile organic compound on Pt-WO_3 enhanced by simple physical mixing with TiO_2. *Catal. Commun.* **2020**, *133*, 105831. [CrossRef]
13. Higashimoto, S.; Ushiroda, Y.; Azuma, M. Electrochemically assisted photocatalysis of hybrid WO_3/TiO_2 films: Effect of the WO_3 structures on charge separation behavior. *Top. Catal.* **2008**, *47*, 148–154. [CrossRef]
14. Tomita, O.; Otsubo, T.; Higashi, M.; Ohtani, B.; Abe, R. Partial oxidation of alcohols on visible-light-responsive WO3 photocatalysts loaded with palladium oxide cocatalyst. *ACS Catal.* **2016**, *6*, 1134–1144. [CrossRef]
15. Niwa, S.; Eswaramoorthy, M.; Nair, J.; Raj, A.; Ito, N.; Shoji, H.; Nanba, T.; Mizukami, F. A one-step conversion of benzene to phenol with a palladium membrane. *Science* **2002**, *295*, 105–107. [CrossRef]
16. Tanev, P.T.; Chibwe, M.; Pinnavaia, T.J. Titanium-containing mesoporous molecular sieves for catalytic oxidation of aromatic compounds. *Nature* **1994**, *368*, 321–323. [CrossRef]
17. Chen, J.; Gao, S.; Xu, J. Direct hydroxylation of benzene to phenol over a new vanadium-substituted phosphomolybdate as a solid catalyst. *Catal. Commun.* **2008**, *9*, 728–733. [CrossRef]
18. Ohkubo, K.; Kobayashi, T.; Fukuzumi, S. Direct oxygenation of benzene to phenol using quinolinium ions as homogeneous photocatalysts. *Angew. Chem. Int. Ed.* **2011**, *50*, 8652–8655. [CrossRef]
19. Fukuzumi, S.; Ohkubo, K. One step selective hydroxylation of benzene to phenol. *Asian J. Org. Chem.* **2015**, *4*, 836–845. [CrossRef]
20. Han, J.W.; Jung, J.; Lee, Y.M.; Nam, W.; Fukuzumi, S. Photocatalytic oxidation of benzene to phenol using dioxygen as an oxygen source and water as an electron source in the presence of a cobalt catalyst. *Chem. Sci.* **2017**, *8*, 7119–7125. [CrossRef]
21. Fukuzumi, S.; Lee, Y.M.; Nam, W. Photocatalytic oxygenation reactions using water and dioxygen. *ChemSusChem* **2019**, *12*, 3931–3940. [CrossRef] [PubMed]
22. Yoshida, H.; Yuzawa, H.; Aoki, M.; Otake, K.; Itoh, H.; Hattori, T. Photocatalytic hydroxylation of aromatic ring by using water as an oxidant. *Chem. Commun.* **2008**, *38*, 4634–4636. [CrossRef] [PubMed]
23. Bui, T.D.; Kimura, A.; Ikeda, S.; Matsumura, M. Determination of oxygen sources for oxidation of benzene on TiO_2 photocatalysts in aqueous solutions containing molecular oxygen. *J. Am. Chem. Soc.* **2010**, *132*, 8453–8458. [CrossRef] [PubMed]
24. Ide, Y.; Matsuoka, M.; Ogawa, M. Efficient visible-light-induced photocatalytic activity on gold-nanoparticle-supported layered titanate. *J. Am. Chem. Soc.* **2010**, *47*, 16762–16764. [CrossRef]
25. Ide, Y.; Torii, M.; Sano, T. Layered silicate as an excellent partner of a TiO_2 photocatalyst for efficient and selective green fine-chemical synthesis. *J. Am. Chem. Soc.* **2013**, *135*, 11784–11786. [CrossRef]
26. Zheng, Z.; Huang, B.; Qin, X.; Zhang, X.; Dai, Y.; Whangbo, M.-H. Facile *in situ* synthesis of visible-light plasmonic photocatalysts M@TiO_2 (M = Au, Pt, Ag) and evaluation of their photocatalytic oxidation of benzene to phenol. *J. Mater. Chem.* **2011**, *21*, 9079–9087. [CrossRef]
27. Goto, T.; Ogawa, M. Efficient photocatalytic oxidation of benzene to phenol by metal complex-clay/TiO_2 hybrid photocatalyst. *RSC Adv.* **2016**, *6*, 23794–23797. [CrossRef]
28. Tomita, O.; Abe, R.; Ohtani, B. Direct synthesis of phenol from benzene over platinum-loaded tungsten(VI) oxide photocatalysts with water and molecular oxygen. *Chem. Lett.* **2011**, *40*, 1405–1407. [CrossRef]

29. Tomita, O.; Ohtani, B.; Abe, R. Highly selective phenol production from benzene on a platinum-loaded tungsten oxide photocatalyst with water and molecular oxygen: Selective oxidation of water by holes for generating hydroxyl radical as the predominant source of the hydroxyl group. *Catal. Sci. Technol.* **2014**, *4*, 3850–3860. [CrossRef]
30. Chen, C.W.; Tano, D.; Akashi, M. Synthesis of platinum colloids sterically stabilized by poly(*N*-vinylformamide) or poly(*N*-vinylalkylamide) and their stability towards salt. *Colloid Polym. Sci.* **1999**, *277*, 488–493. [CrossRef]
31. Arabatzis, I.M.; Stergiopoulos, T.; Andreeva, D. Characterization and photocatalytic activity of Au/TiO_2 thin films for azo-dye degradation. *J. Catal.* **2003**, *220*, 127–135. [CrossRef]
32. Buchachenko, A.L.; Dubinina, E.O. Photo-oxidation of water by molecular oxygen: Isotope exchange and isotope effects. *J. Phys. Chem. A* **2011**, *115*, 3196–3200. [CrossRef] [PubMed]
33. Pourbaix, M. *Atlas of Electrochemical Equilibria in Aqueous Solutions*; Pergamon Press Ltd.: London, UK, 1966.
34. Panchenko, A.; Koper, M.T.M.; Shunbina, T.E.; Mitchell, S.J.; Roduner, E. *Ab Initio* calculation of intermediates of oxygen reduction on low-index platinum surfaces. *J. Electrochem. Soc.* **2004**, *151*, A2016–A2027. [CrossRef]
35. Frisch, M.J.; Trucks, G.W.; Schlegel, H.B.; Scuseria, G.E.; Robb, M.A.; Cheeseman, J.R.; Scalmani, G.; Barone, V.; Mennucci, B.; Petersson, G.A.; et al. *Gaussian 09*; Revision D.01; Gaussian, Inc.: Wallingford, CT, USA, 2013.
36. Becke, A.D. A new mixing of Hartree–Fock and local density-functional theories. *J. Chem. Phys.* **1993**, *98*, 5648–5652. [CrossRef]
37. Hay, P.J.; Wadt, W.R. Ab initio effective core potentials for molecular calculations. Potentials for the transition metal atoms Sc to Hg. *J. Chem. Phys.* **1985**, *82*, 270–283. [CrossRef]
38. Dunning, T.H.; Hay, P.J.; Schaefer, H.F. *Modern Theoretical Chemistry*; Schaefer, H.F., III, Ed.; Plenum Press: New York, NY, USA, 1976; Volume 3, pp. 1–28.
39. Fukui, K.; Kato, S.; Fujimoto, H. Constituent analysis of the potential gradient along a reaction coordinate. Method and an application to methane + tritium reaction. *J. Am. Chem. Soc.* **1975**, *97*, 1–7. [CrossRef]